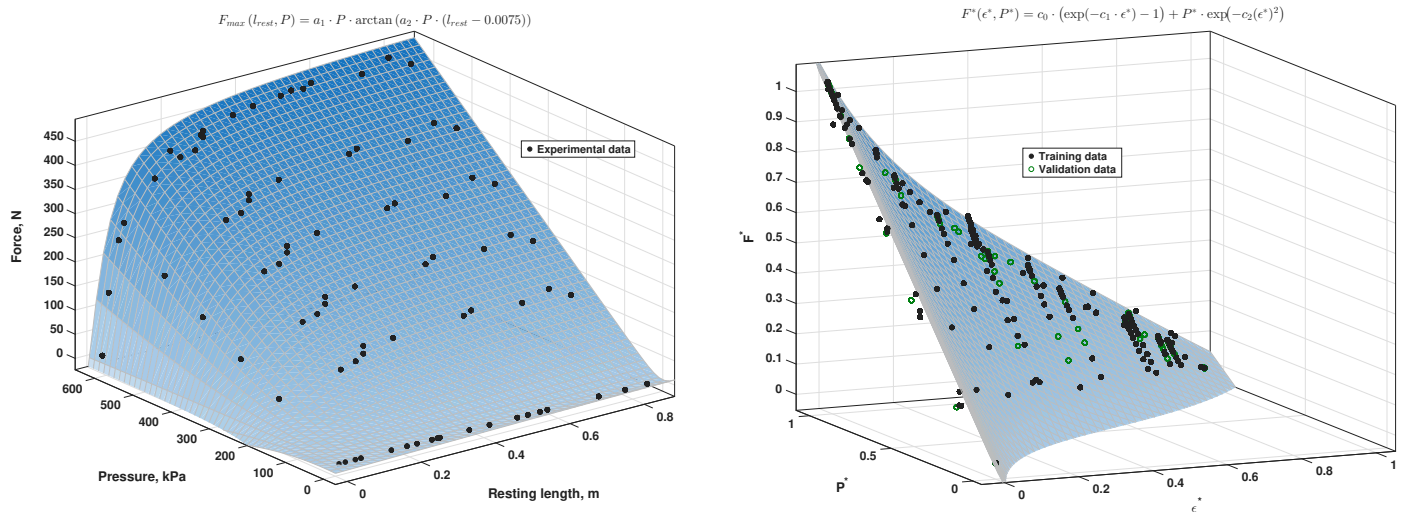


Graphical Abstract

Isometric Force Characterization of Braided Pneumatic Actuators

Ben Bolen^①, Mohamad Elzein^②, Lawrence Pang, Alexander J. Hunt^③



Highlights

Isometric Force Characterization of Braided Pneumatic Actuators

Ben Bolen^①, Mohamad Elzein^②, Lawrence Pang, Alexander J. Hunt^③

- Braided Pneumatic Actuator maximum isometric force is a function of resting length
- Force curves are normalized with pressure and maximum contraction
- A high-fidelity predictive force model is developed using few coefficients

Isometric Force Characterization of Braided Pneumatic Actuators

Ben Bolen^{①,a,*}, Mohamad Elzein^{①,a}, Lawrence Pang^a, Alexander J. Hunt^{①,a}

^a*Department of Mechanical and Materials Engineering, Portland State University, PO Box 751, 97207-0751, OR, USA*

Abstract

Artificial muscles such as braided pneumatic actuators (BPAs) offer many advantages for robotic systems, including high durability and strength-to-weight ratios. However, their use in robotic systems is still extremely limited, in part due to their poor force, length, and pressure characterization. In this work, a test setup is created to compare force produced by Festo fluidic BPAs with leading models. Our analysis of the data has resulted in 1) the development of new equations to calculate force as functions of pressure and contraction for Festo BPAs with uninflated diameters (ϕ) of 10 mm and 20 mm, and 2) a novel equation for the maximum force in 10 mm and 20 mm diameter Festo BPAs as a function of their resting length (l_{rest}). This will lead to faster design processes and the development of new systems such as biomimetic robots that are able to more accurately reproduce the range of motion and isometric torque profiles that exist in the animals they are mimicking.

Keywords: BPA, Biomimetic, Function Fit, PAM, Artificial Muscle, Isometric Force

1. Introduction

Biomimetic robots provide a platform for investigating how mechanical structure and control interact to generate movement, offering complementary insights to simulation-based studies (Andrews, 1985; Millard et al., 2013; Arnold et al., 2010). Musculoskeletal humanoids and limb systems driven by tendon-like actuators have been shown to support biologically meaningful experiments on motion generation, internal force transmission, and neural control hypotheses (Asano et al., 2017, 2019; Hitzmann et al., 2018; Liu et al., 2018; Chen et al., 2019). This dual perspective of using robots to learn about biology and using biology to design more adaptive robots has been emphasized in both biomimetic robotics and biomechanics (Ijspeert, 2020; Asano et al., 2017).

A wide range of actuation technologies have been explored in robotics, including electric motors, hydraulic systems, smart-material actuators, and artificial muscles (He and Gao, 2020; Liang et al., 2020). Electric motors are widely used due to their controllability and maturity, but are limited by thermal constraints, gearing requirements, and reduced compliance compared to muscle-like actuators (Veale and Xie, 2016; Suzumori and Faudzi, 2018). Hydraulic actuators offer exceptionally high power density and have enabled highly dynamic legged systems, but they remain relatively heavy, less efficient than biological muscle, and require a dedicated fluid infrastructure (Suzumori and Faudzi, 2018). Dielectric elastomer actuators (DEAs), a class of electronic electroactive polymers, demonstrate high specific work and good bandwidth in comparative studies (Liang et al., 2020). However, they are limited by the need for kilovolt-range driving voltages (Madden et al., 2004), electromechanical

instability, and the requirement for compliant electrodes (Liang et al., 2020). In contrast, McKibben-style braided pneumatic actuators (BPAs) combine low mass, high force-to-weight ratio, and intrinsic compliance with a force-length curve that qualitatively resembles that of skeletal muscle (Liang et al., 2020; Hunt et al., 2017). BPAs have been used in quadrupedal robots (Aschenbeck et al., 2006; Hunt et al., 2017), musculoskeletal humanoids (Asano et al., 2017; Hitzmann et al., 2018), and dexterous manipulation systems (Chen et al., 2019), demonstrating their ability to support biologically motivated investigations and improve robot adaptability in unstructured environments.

Despite these advantages, BPAs exhibit several important differences from biological muscle. First, BPA maximum tensile force occurs at resting (i.e., uninflated) length (l_{rest}) rather than at an optimal fiber length (Liang et al., 2020). Second, their maximum contraction ratio is substantially lower than that of human muscle, presenting challenges for achieving biomimetic joint ranges of motion (Hunt et al., 2017; Sárosi et al., 2017; Liang et al., 2020). Third, BPAs have a highly nonlinear dependence on internal pressure (P), contraction (ϵ), and loading state (Hunt et al., 2017; Martens and Boblan, 2017), which complicates control and motivates high-fidelity force-length-pressure modeling.

To address these challenges, numerous researchers have proposed static and dynamic models for BPAs. Sárosi et al. (2017) compared geometric and empirical models for uninflated diameters (ϕ) 10 mm and 20 mm actuators and highlighted limitations when l_{rest} varies. Martens and Boblan (2017) introduced a physically motivated static model for the Festo DMSP series and demonstrated accurate predictions at specific l_{rest} . Festo provides a manufacturer tool for predicting force as a function of pressure and contraction (Festo, 2022; Lang, 2005), but experimental comparisons indicate that it does not adequately account for variation in l_{rest} or actuator-specific contraction limits. Hunt

*Corresponding author

Email address: bbolen83@gmail.com (Ben Bolen)

et al. (2017) developed a more generalizable empirical model for ϕ 10 mm Festo BPAs that incorporates differences between eccentric and concentric loading states and accounts for the maximum achievable contraction (ϵ_{max}) at high pressures. Comparisons with experimental data indicates that none of the existing models effectively takes into account differences in maximum force due to initial actuator length.

The present work develops an improved force–pressure–length model for both ϕ 10 mm and ϕ 20 mm Festo BPAs. We collected extensive force data for a wide range of resting lengths, contraction ratios, and internal pressures. These data were first used to find maximum force as a function of resting length. Then we normalized the data to formulate normalized force (F^*) as a function of relative strain (ϵ^*) and relative pressure (P^*). The resulting model provides improved predictive accuracy for isometric BPA force, supporting the design and control of biomimetic robotic systems that rely on BPAs.

2. Background

Previous studies have generated empirical models of the force-length-pressure relationship of BPA actuators. Sárosi et al. (2017) discuss several high-fidelity BPA force models. They present a static force model with a 21 coefficient polynomial function for a Festo MAS-20-200N (i.e. ϕ 20 mm, $l_{rest} = 200$ mm) with an impressive $R^2 = 0.9994$. They also present Sárosi's static force model for a Festo DMSP-20-400N-RM-RM (i.e. ϕ 20 mm, $l_{rest} = 400$ mm), with 6 coefficients and a $R^2 = 0.9995$. Martins and Boblan present an even more accurate model, in terms of absolute error, using five coefficients for a DMSP-10-250 (i.e. ϕ 10 mm, $l_{rest} = 250$ mm) and a DMSP-20-300 (i.e. ϕ 20 mm, $l_{rest} = 300$ mm) (Martens and Boblan, 2017). However, our work, as presented below, demonstrates that different resting lengths produce different force-length curves, preventing the use of these models for designing systems with different resting lengths.

Hunt et al. (2017) looked at six resting lengths of ϕ 10 mm Festo BPAs, accounting for differences in maximum contractile percentages, and elucidating the force-length-pressure relationship. In particular, for a given contraction percent and force F (in Newtons), the scalar pressure P (in kPa) required to produce this force for a ϕ 10 mm Festo artificial muscle can be determined by solving the equation:

$$P = 254 \text{ kPa} + F \cdot 1.23 \text{ kPa N}^{-1} + S \cdot 15.6 \text{ kPa} + 192 \text{ kPa} \cdot \tan\left(2.03 \left(\frac{\epsilon}{\epsilon_{max}} - F \cdot 0.331 \times 10^{-3} \text{ N}^{-1}\right) - 0.46\right) \quad (1)$$

where S is the artificial muscle hysteresis factor such that $S = 1$ indicates the muscle is shortening, $S = -1$ indicates it is lengthening, and $S = 0$ under static conditions. An important note for Eq. 1 is that the coefficients have been updated with the correct values as the values reported in Hunt et al. (2017) contained typographical errors. The amount of contraction, ϵ , is calculated as

$$\epsilon = \frac{(l_{rest} - l)}{l_{rest}} \quad (2)$$

where ϵ_{620} is the amount of contraction in a BPA without external load when inflated at 620 kPa (90 psi), similarly calculated as

$$\epsilon_{620} = \frac{(l_{rest} - l_{620})}{l_{rest}} \quad (3)$$

where l_{620} is defined as the muscle length measured at 620 kPa. Eq. 1 was used to create a lookup table for actuator force, F , for a given amount of pressure, P , and relative contraction, ϵ^* , defined as

$$\epsilon^* = \frac{\epsilon}{\epsilon_{620}} \quad (4)$$

using the results from Eq. 2 and Eq. 3.

However, this model was taken at low forces (≤ 24 lbs), and it is unclear how well this model captures actuator behavior at higher forces, so we compare this model with data collected in this work.

3. Methods and Materials

3.1. Overview

To measure artificial muscle force as a function of length and pressure, we built a test jig from extruded aluminum and 3D printed parts. Festo BPAs with 10 mm and 20 mm diameter were tested with various resting lengths and different amounts of contraction. These data are used to develop an improved model that more accurately predicts maximum muscle force based on l_{rest} , current muscle length l_m , and pressure P . The results are compared with existing models and the new data is used to create an updated model.

3.2. BPA force characterization experiment

A test jig was made of 80/20® brand 1515 series extruded aluminum (Fig. 1). Artificial muscles were placed vertically in the jig one at a time. The upper end was attached to an S-shaped load cell. The lower end was attached to an adjustable crossmember that was used to change the actuator length l_m . Compressed air was supplied through the building at 620 kPa and measured with a Freescale MPX5700 pressure sensor.

The inner distance between the hose clamps on each BPA was measured to determine the muscle's resting length (l_{rest}). This is how Festo (2022) defines l_{rest} , although in Hunt et al. (2017) it was measured to also include end cap length. We then inflated each BPA to $P_{620} = 620$ kPa, with one end allowed to move freely in the axial Degree of Freedom (DoF), and measured the length l_{620} to calculate maximum contraction at 620 kPa using Eq. 3. The distance between the crossmembers was then controlled to obtain different amounts of contraction, the muscles were inflated to various pressures, and the contractile force was recorded at the pressure-contraction pairs. This was done for ϕ 10 mm BPA resting lengths (l_{rest}) of 112 mm – 518 mm. For ϕ 20 mm BPAs, resting lengths (l_{rest}) of 300 mm – 509 mm were used.

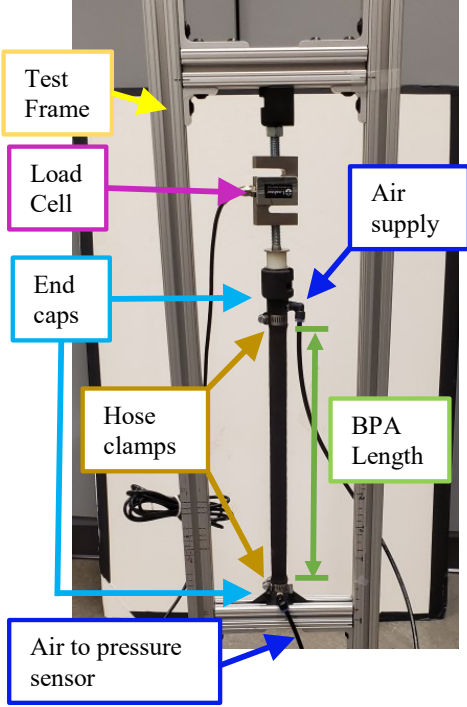


Figure 1: A picture of a BPA in the isometric force test stand with components labeled.

4. Results

4.1. Maximum Force at 620 kPa

Data of the maximum force from BPA characterization tests of the 10 mm and 20 mm diameters at 620 kPa show a dependency on resting length (Fig. 2). This is a previously unreported characteristic of these artificial muscles. Detailed analysis of the Festo Tool (Festo, 2022), do in fact predict a change in maximum force with the resting length, however the Festo Tool predicts increased force with shorter lengths, while our collected data indicate decreasing force with shorter lengths. The data show a force response resembling an arctan curve along the l_{rest} dimension. Using the Nonlinear Least Squares method and a Least Absolute Residual robustness, we fit an arctan curve to the data to get the maximum force at 620 kPa given a resting length as:

$$F_{620_{10}} = 303.5 \text{ N} \cdot \arctan(19.03 \text{ m}^{-1} \cdot (l_{rest} - 0.0075)) \quad (5)$$

$$F_{620_{20}} = 922.4 \text{ N} \cdot \arctan(15.37 \text{ m}^{-1} \cdot (l_{rest} - 0.013)) \quad (6)$$

The length is offset by 0.0075 m and 0.013 m because solid modeling showed that the end caps contact each other at these lengths. At these lengths, the actuator would not be able to contract to produce force.

4.2. Force as a function of pressure and resting length

Data from BPA characterization tests of the 10 mm muscles resulted in force-pressure pairings for different muscle resting

lengths (l_{rest}) (Fig. 3A). Similar to the maximum force data, these data show a force response resembling an arctan curve along the l_{rest} dimension with a more linear response to changes in pressure. Using the Nonlinear Least Squares method and a Least Absolute Residual robustness, we fit an arctan curve to the data to get the maximum force given a resting length and pressure as:

$$F_{max}(l_{rest}, P) = a_1 \cdot P \cdot \arctan(a_2 \cdot P \cdot (l_{rest} - 0.0075)) \quad (7)$$

where $a_1 = 0.4895 \text{ N kPa}^{-1}$ and $a_2 = 0.03068 \text{ kPa}^{-1} \text{ m}^{-1}$ for the 10 mm actuator, and $a_1 = 1.49 \text{ N kPa}^{-1}$, $a_2 = 0.0248 \text{ kPa}^{-1} \text{ m}^{-1}$ for the 20 mm actuator. Goodness-of-fit measures are given in Table 1 in the appendix.

4.3. Maximum Contraction at 620 kPa

Fig. 3B shows an attempt at a linear fit for maximum contraction at 620 kPa (ϵ_{620}) as a function of resting length (l_{rest}). There was a large amount of variance in the data, with the linear fit giving an adjusted $R^2 = 0.4124$ and an RMSE = 0.0083. Since there is no direct, predictable relationship between maximum contraction and l_{rest} , this value should be recorded in each muscle used on a robot to best predict the force it may produce at different pressures and contraction.

4.4. Force as a function of pressure and contraction

In addition to being a function of the pressure and resting length, the force produced by the actuator is also a function of the amount of actuator contraction, with less force being applied as the actuator contracts. To build this model, the collected data of force, pressure, and contraction are normalized by dividing by F_{620} , P_{620} , and ϵ_{620} , respectively. This had the effect of compressing the data into a 3D surface ranging from 0 to 1 on all axes. Normalized data are compared with pressure isolines of force predicted by the Festo tool divided by the maximum force equation described in the previous section (Fig. 4). With this comparison, it is clear that the Festo tool over-predicts the expected force, especially at lower pressures and contraction.

We therefore derived our own equation for isometric force in the BPA as a function of pressure and contraction. Visual analysis of the experimental data shows an exponential relationship between ϵ^* and F^* , and a linear relationship between P^* and F . We fit a surface to the data using nonlinear least squares and a least absolute residual robustness such that:

$$F^*(\epsilon^*, P^*) = \begin{cases} c_0 \cdot (\exp(-c_1 \cdot \epsilon^*) - 1) + \\ P^* \cdot \exp(-c_2(\epsilon^*)^2) & \text{for } F^* > 0 \\ 0 & \text{for } F^* \leq 0 \end{cases} \quad (8)$$

For the $\phi 10$ mm BPAs, the result of the improved fit can be seen in Figure 4A. The adjusted $R^2 = 0.9998$, a RMSE = 0.004537, and a maximum absolute residual of 10.6%. Solving 8 for the $\phi 20$ mm BPA, yields different coefficients, and results are seen in Fig. 4B. Coefficient values and goodness of fit statistics are found in table 2.

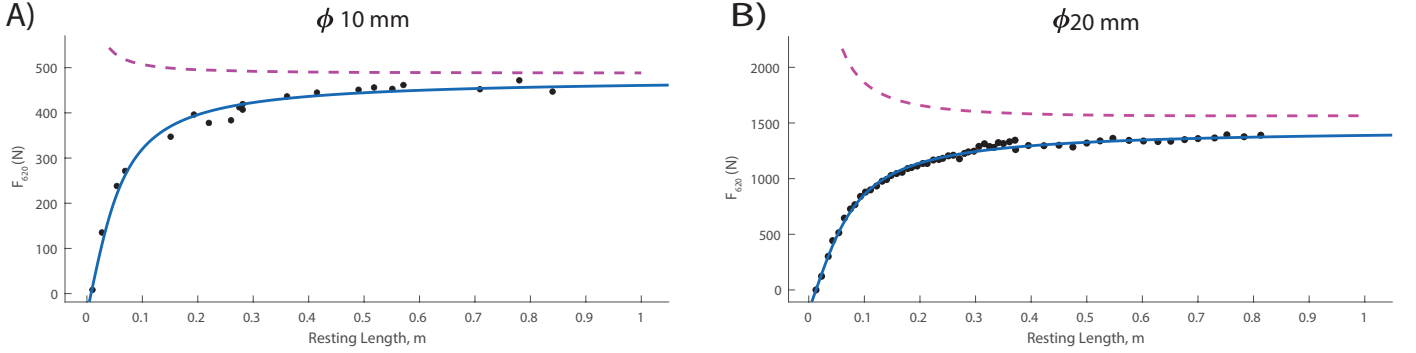


Figure 2: Results for finding the relationship between F_{620} and l_{rest} . **(A)** $F_{620_{10}}$ as a function of l_{rest} , at P_{620} . Dashed line is the $F_{620_{10}}$ data from Festo. Solid line is the fit from equation 5. **(B)** $F_{620_{20}}$ as a function of l_{rest} at P_{620} . Dashed line is $F_{620_{20}}$ data from Festo. Solid line is the fit from equation 6.

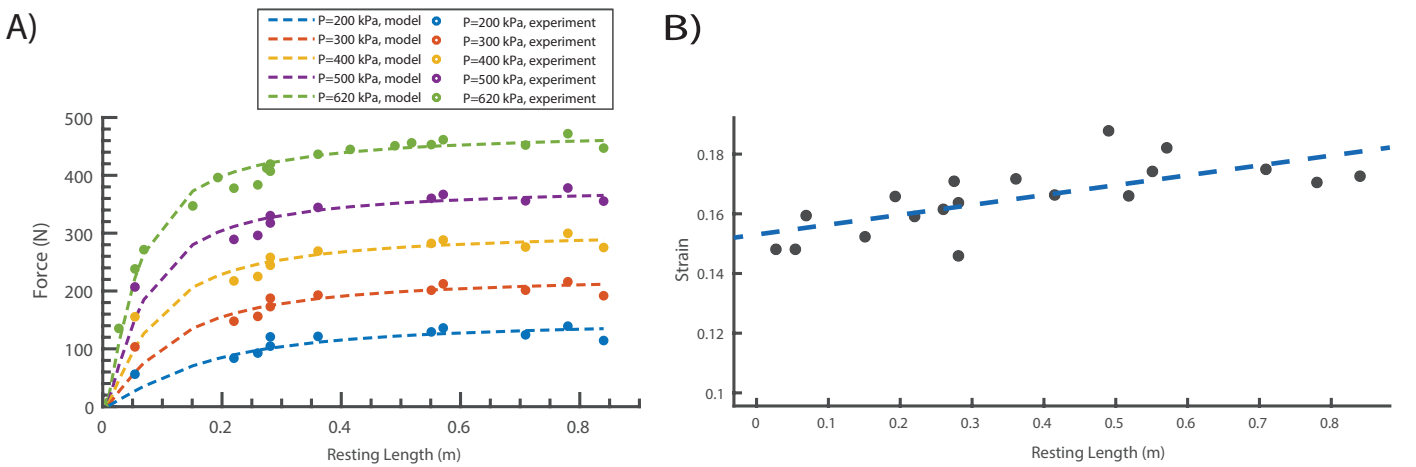


Figure 3: Results for finding the relationship between F_{620} , l_{rest} , P_{620} , and ϵ_{620} . **(A)** Isoclines of the surface fit for $F_{620_{10}}(l_{rest}, P_{620})$. **(B)** ϵ_{620} versus l_{rest} at P_{620} . Although there is a general trend of longer resting lengths producing more contraction, no conclusive relationship between ϵ_{620} and l_{rest} could be deduced from this experiment.

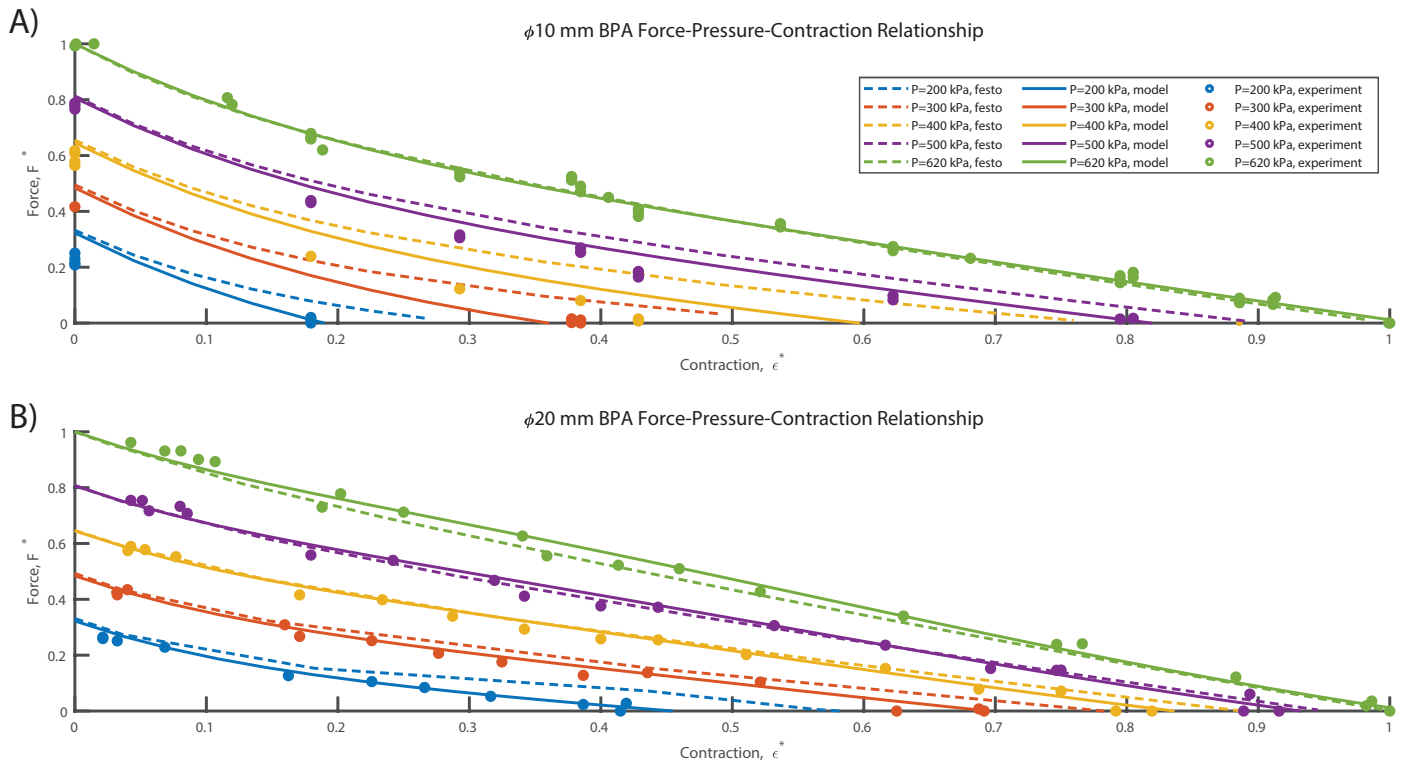


Figure 4: Surface fit for $F^*(\epsilon^*, P^*)$. Solid lines are from our model. Dashed lines from Festo supplied data. In total, 537 data points were collected and used to fit the 3D surfaces (321 data points for $\phi 10$ mm BPAs and 216 data points for $\phi 20$ mm BPAs). 80% of these data were used for training, and 20% were used for validation. For figure clarity, not all data is included and plotted circles represent collected data at ± 10 kPa of the stated pressure. (A) Fit data for $\phi 10$ mm Festo BPAs. (B) Fit data for $\phi 20$ mm Festo BPAs.

5. Discussion

We have developed new F_{620} equations for 10 mm and 20 mm diameter Festo BPAs that capture the change in maximum force produced by the actuators at 620 kPa as a function of their resting length. When examining Eq. 5 and measured data in Fig. 2B, it can be seen that as l_{rest} goes to infinity, $F_{620,10}$ goes to 470 N. When the Festo tool (Lang, 2005) was queried at $l_{rest} = 1$ m as an approximation of infinity, it predicts the $\phi 10$ mm BPA can produce $F = 490$ N at P_{620} . This is within the 10% variability that Festo states may occur in manufacturing tolerances. Similarly, the Festo data predict a $\phi 20$ mm BPA will produce $F = 1570$ N. However, our results for Eq. 6 show that $F_{620,20}$ goes to 1460 N as l_{rest} approaches infinity. Although the difference is much larger, it is also within the 10% manufacturing tolerance.

Where our measured data differs significantly from the Festo model, is that as l_{rest} goes to zero. For the measured data, as the length gets smaller, the force does as well, whereas the Festo tool predicts exponential force increase (see Fig. 2). As a specific example, when specifying $l_{rest} = 112$ mm for the 10 mm diameter BPAs, the Festo predicted F_{620} is 498.6 N. However, using Eq. 5, F_{620} is calculated to be 335.3 N. Actual force in the $l_{rest} = 112$ mm was measured at 350.9 N. Therefore, the error in predicted F_{620} for the $\phi 10$ mm BPA is 4.5% for our model and 42.1% using the Festo tool. Researchers using BPA resting lengths under 300 mm should take note of these results.

It remains to be seen how ϵ_{620} can be known a priori. We still suspect that it is a function of l_{rest} , but it might also be a function of product batch number. Modeling work of ideal McKibben actuators describe how this is a function of the total number of twists, and the angle of twist in the usable muscle area (Chou and Hanaford, 1996). Uncovering this relationship for the Festo DMSP/MAS artificial muscles, if it exists in a meaningful way, will require additional controlled tests. Not knowing this relationship a priori means there is still the potential for robots and other systems to go through an iterative design stage if it is discovered that the system does not produce the torque or have the RoM that the design team expects. However, the data and models provided here should enable for faster redesigns with fewer additional measurements.

We have also introduced the concept of nondimensionalized isometric force that is a function of relative strain and relative pressure (Eq. 8). This elegant equation has only 3 coefficients with low error (Table 2). In the work presented here, we add in the relative pressure term, $P^* = P/P_{620}$. Our data shows that by normalizing force, contraction, and pressure, we are able to create a simplified force equation as a function of contraction and pressure that scales well with initial actuator length, i.e.

$$F(\epsilon^*, P^*, l_{rest}) = F^*(\epsilon^*, P^*) \cdot F_{620}(l_{rest}) \quad (9)$$

For example, given $l_{rest} = 54$ mm and $P = 300$ kPa, the measured force was $F_{actual} = 103$ N. Force prediction using only the Festo tool predicts the force to be $F_{predict} = 270$ N. This is 161% greater than the measured force. Using Eq. 5 and Eq. 8 with Eq. (9) gives $F_{predict} = F^*(0, 0.48) \cdot F_{620}(0.054) = 0.49 \cdot 230$ N = 112 N. This is an error of 8%, which is much more accurate than using the Festo tool only.

In our work, $P_{620} = 620$ kPa is the maximum supply pressure for our system, and other users of this actuator may use a different supply pressure. However, this supply pressure is not required, and normalizing by this value was chosen as a method for improving the optimization techniques by reducing the sensitivity of the term associated with pressure. This equation will work for any pressure supplies below the 620 kPa. We also anticipate the equation will also work for pressures up to 800 kPa (the maximum rated pressure for Festo 10 mm BPAs), however we do not have the data to confirm this.

The improved BPA characterization more accurately predicts isometric force produced by the BPAs. Unlike Eq. 9, it does not account for the hysteresis that occurs in BPAs. BPA artificial muscles are often said to be analogous to biological muscles because they have force length curves and can produce force only in tension. This analogy is worth closer inspection, although it should be kept in mind that biological muscle optimum fiber length l_{OFL} is not equivalent to l_{rest} . The improved Hill-muscle model of Thelen (2003) shows an exponential term for a muscle's passive force-length property concentric loading.

The analysis in this study has created novel equations for calculating force in Festo 10 mm and 20 mm diameter BPAs. This study has elucidated the relationship between maximum BPA force at 620 kPa F_{620} as a function of resting length l_{rest} (Eq. 5, Eq. 6, Table 1). We have also created more accurate equations for the nondimensionalized force in a BPA as a function of relative strain ϵ^* and relative pressure P^* , (Eq. 8 and Table 2). Taken together, the $F_{620}(l_{rest})$ fits and the nondimensional force surface $F^*(\epsilon^*, P^*)$ provide a practical way to predict isometric BPA force across resting lengths using a small number of measurements. In a design workflow, these equations make it easier to select actuator diameter and resting length, and to evaluate whether a proposed routing can meet force and range-of-motion requirements before committing to a full prototype. As a result, BPA-driven mechanisms (e.g., joints in biomimetic legs or manipulators) can be developed with fewer design iterations and with realistic expectations of force output at short resting lengths.

Resource Identification Initiative

- MATLAB (RRID:SCR_001622)
- Arduino UNO (RRID:SCR_017284)

Conflict of Interest Statement

The authors declare that the research was conducted in the absence of any commercial or financial relationships that could be construed as a potential conflict of interest.

Author Contributions

BB and AH contributed to the conception and design of the study. BB and CM wrote the code to calculate theoretical isometric torque values of the robot. Figures were created by

BB and AH. BB, LP, and ME wrote code for data collection and analysis. BB, LP, and ME collected the data. BB performed the statistical analysis and organized the database. BB wrote the first draft of the manuscript. BB and AH wrote sections of the manuscript. All authors read the manuscript, contributed to its revision, and approved the submitted version.

Funding

Research for this article was funded by the Department of Mechanical and Materials Engineering at Portland State University, the National Science Foundation (NSF) grant for NeuroNex: Communication, Coordination, and Control in Systems (C3NS) 2015317 and NSF grant 1943483.

Acknowledgments

The authors would like to thank Jasmine Bradley for her help reworking the figures in the results section. As a visual designer, her contributions improved the aesthetic quality of the images and ensured data accessibility for people with color blindness. Furthermore, the authors would like to express their gratitude towards Cody Scharzenberger for all his assistance in proof-reading and editing the manuscript.

Data Availability Statement

The data sets are available from the authors upon reasonable request.

References

- Andrews, J.G., 1985. A General Method for Determining the Functional Role of a Muscle. *Journal of Biomechanical Engineering* 107, 348–353. URL: <https://doi.org/10.1115/1.3138568>, doi:10.1115/1.3138568.
- Arnold, E.M., Ward, S.R., Lieber, R.L., Delp, S.L., 2010. A Model of the Lower Limb for Analysis of Human Movement. *Annals of Biomedical Engineering* 38, 269–279. URL: <http://link.springer.com/10.1007/s10439-009-9852-5>, doi:10.1007/s10439-009-9852-5.
- Asano, Y., Okada, K., Inaba, M., 2017. Design principles of a human mimetic humanoid: Humanoid platform to study human intelligence and internal body system. *Science Robotics* 2. URL: <https://robotics.sciencemag.org/content/2/13/eaq0899>, doi:10.1126/scirobotics.aq0899. publisher: Science Robotics Section: Research Article.
- Asano, Y., Okada, K., Inaba, M., 2019. Musculoskeletal design, control, and application of human mimetic humanoid Kenshiro. *Bioinspiration & Biomimetics* 14, 036011. URL: <https://iopscience.iop.org/article/10.1088/1748-3190/ab03fc>, doi:10.1088/1748-3190/ab03fc.
- Aschenbeck, K., Kern, N., Bachmann, R., Quinn, R., 2006. Design of a Quadruped Robot Driven by Air Muscles, in: The First IEEE/RAS-EMBS International Conference on Biomedical Robotics and Biomechatronics, 2006. BioRob 2006., pp. 875–880. URL: <https://ieeexplore.ieee.org/abstract/document/1639201>, doi:10.1109/BIOROB.2006.1639201. iSSN: 2155-1782.
- Chen, J., Zhong, S., Kang, E., Qiao, H., 2019. Realizing human-like manipulation with a musculoskeletal system and biologically inspired control scheme. *Neurocomputing* 339, 116–129. URL: <https://www.sciencedirect.com/science/article/pii/S0925231218315315>, doi:10.1016/j.neucom.2018.12.069.
- Chou, C.P., Hannaford, B., 1996. Measurement and modeling of McKibben pneumatic artificial muscles. *IEEE Transactions on Robotics and Automation* 12, 90–102. URL: <https://ieeexplore.ieee.org/document/481753/>, doi:10.1109/70.481753.
- Festo, 2022. Festo Fluidic Muscle DMSP. URL: <https://www.festo.com/media/pim/556/D15000100140556.PDF>.
- He, J., Gao, F., 2020. Mechanism, Actuation, Perception, and Control of Highly Dynamic Multilegged Robots: A Review. *Chinese Journal of Mechanical Engineering* 33, 79. URL: <https://doi.org/10.1186/s10033-020-00485-9>, doi:10.1186/s10033-020-00485-9.
- Hitzmann, A., Masuda, H., Ikemoto, S., Hosoda, K., 2018. Anthropomorphic musculoskeletal 10 degrees-of-freedom robot arm driven by pneumatic artificial muscles. *Advanced Robotics* 32, 865–878. URL: <http://stats.lib.pdx.edu/proxy.php?url=http://search.ebscohost.com/login.aspx?direct=true&db=aph&AN=131926820&site=ehost-live>, doi:10.1080/01691864.2018.1494040. publisher: Taylor & Francis Ltd.
- Hunt, A., Gruber-Tilton, A., Quinn, R., 2017. Modeling length effects of braided pneumatic actuators, in: Volume 5A: 41st Mechanisms and Robotics Conference, ASME, Cleveland, OH. p. V05AT08A008. URL: <https://asme.pinetec.com/detc2017/data/pdfs/trk-8/DETC2017-67458.pdf>, doi:10.1115/detc2017-67458.
- Ijspeert, A.J., 2020. Amphibious and Sprawling Locomotion: From Biology to Robotics and Back. *Annual Review of Control, Robotics, and Autonomous Systems* 3, 173–193. URL: <https://doi.org/10.1146/annurev-control-091919-095731>, doi:10.1146/annurev-control-091919-095731. eprint: <https://doi.org/10.1146/annurev-control-091919-095731>.
- Lang, R., 2005. Festo MuscleSim. URL: https://www.festo.com/net/en-us_us/SupportPortal/Details/7942/Document.aspx or <http://www.festo.com>.

- Liang, W., Liu, H., Wang, K., Qian, Z., Ren, L., Ren, L., 2020. Comparative study of robotic artificial actuators and biological muscle. *Advances in Mechanical Engineering* 12, 1687814020933409. URL: <https://doi.org/10.1177/1687814020933409>, doi:10.1177/1687814020933409. publisher: SAGE Publications.
- Liu, X., Rosendo, A., Ikemoto, S., Shimizu, M., Hosoda, K., 2018. Robotic investigation on effect of stretch reflex and crossed inhibitory response on bipedal hopping. *Journal of the Royal Society Interface* 15, 20180024. doi:10.1098/rsif.2018.0024. place: London Publisher: Royal Soc WOS:000428576200018.
- Madden, J., Vandesteeg, N., Anquetil, P., Madden, P., Takshi, A., Pytel, R., Lafontaine, S., Wieringa, P., Hunter, I., 2004. Artificial muscle technology: physical principles and naval prospects. *IEEE Journal of Oceanic Engineering* 29, 706–728. doi:10.1109/JOE.2004.833135. conference Name: IEEE Journal of Oceanic Engineering.
- Martens, M., Boblan, I., 2017. Modeling the Static Force of a Festo Pneumatic Muscle Actuator: A New Approach and a Comparison to Existing Models. *Actuators* 6, 33. URL: <http://www.mdpi.com/2076-0825/6/4/33>, doi:10.3390/act6040033.
- Millard, M., Uchida, T., Seth, A., Delp, S.L., 2013. Flexing Computational Muscle: Modeling and Simulation of Musculotendon Dynamics. *Journal of Biomechanical Engineering* 135, 021005. URL: <https://asmedigitalcollection.asme.org/biomechanical/article/doi/10.1115/1.4023390/371394/Flexing-Computational-Muscle-Modeling-and>, doi:10.1115/1.4023390.
- Suzumori, K., Faudzi, A.A., 2018. Trends in hydraulic actuators and components in legged and tough robots: a review. *Advanced Robotics* 32, 458–476. URL: <https://doi.org/10.1080/01691864.2018.1455606>, doi:10.1080/01691864.2018.1455606. publisher: Taylor & Francis _eprint: <https://doi.org/10.1080/01691864.2018.1455606>.
- Sárosi, J., Pitel', J., Tóthová, M., Hošovský, A., Bíró, I., 2017. COMPARATIVE SURVEY OF VARIOUS STATIC AND DYNAMIC MODELS OF PNEUMATIC ARTIFICIAL MUSCLES. *Transactions of the Canadian Society for Mechanical Engineering* 41, 825–844. URL: <http://www.nrcsearchpress.com/doi/10.1139/tcsme-2017-514>, doi:10.1139/tcsme-2017-514.
- Thelen, D.G., 2003. Adjustment of Muscle Mechanics Model Parameters to Simulate Dynamic Contractions in Older Adults. *Journal of Biomechanical Engineering* 125, 70–77. URL: <https://asmedigitalcollection.asme.org/biomechanical/article/125/1/70/463793/Adjustment-of-Muscle-Mechanics-Model-Parameters-to>, doi:10.1115/1.1531112.
- Veale, A.J., Xie, S.Q., 2016. Towards compliant and wearable robotic orthoses: A review of current and emerging actuator technologies. *Medical Engineering & Physics* 38, 317–325. URL: <https://www.sciencedirect.com/science/article/pii/S135045331600031X>, doi:10.1016/j.medengphy.2016.01.010.

Tables

Table 1: Maximum force equation coefficient values with confidence intervals (CI) and goodness-of-fit measures. Eq. 7 is compared to data taken at 620 kPa . Eq. 5 and Eq. 6 are compared against maximum force from using the Festo tool. It was not necessary to fit an adjusted R² in these cases.

Equation	Coefficient	CI (95%)	Model			Comparison		
			Adj. R ²	RMSE	Max. Error	Adj. R ²	RMSE	Max. Error
(7)	$a_1 = 0.4895 \text{ N kPa}^{-1}$	(0.4822, 0.4968)	0.9945	11.61 N	55.3 N	0.9854	14.7 N	30.9 N
	$a_2 = 0.03068 \text{ kPa}^{-1} \text{ m}^{-1}$	(0.0282, 0.03317)						
(5)	$b_1 = 303.5 \text{ N}$	(300, 308)	0.9854	14.72 N	30.9 N	–	189.9 N	375.6 N
	$b_2 = 19.03 \text{ m}^{-1}$	(17.48, 20.57)						
(6)	$b_1 = 922.4 \text{ N}$	(914.2, 930.7)	0.9945	23.83 N	62.1 N	–	668.4 N	1590.1 N
	$b_2 = 15.37 \text{ m}^{-1}$	(14.75, 15.98)						

Table 2: Normalized isometric BPA force equation (Eq. 8) coefficient values and goodness-of-fit measures.

BPA	Coefficient	CI (95%)	Model			Validation		
			Adj. R ²	RMSE	Max. Error	Adj. R ²	RMSE	Max. Error
$\phi 10 \text{ mm}$	$c_0 = 0.5682$	(0.5584, 0.578)	0.9998	0.005118	10.3%	0.9994	0.0245409	10.6%
	$c_1 = 4.254$	(4.126, 4.383)						
	$c_2 = 0.5597$	(0.5429, 0.5766)						
$\phi 20 \text{ mm}$	$c_0 = 0.2579$	(0.2401, 0.2756)	0.992	0.02294	6.8%	0.9943	0.0231303	5.7%
	$c_1 = 6.477$	(5.558, 7.396)						
	$c_2 = 1.321$	(1.239, 1.403)						